Supplemental Materials

Molecular Biology of the Cell

Gonzalez et al.

Materials and Methods

Cell Culture. NIH 3T3 fibroblasts were a gift from D. Wirtz (Johns Hopkins University, Baltimore, MD), neonatal foreskin fibroblasts (NuFF) were a gift from S. Gerecht (Johns Hopkins University, Baltimore, MD) and mouse Mesenchymal Stem Cells were a gift from Xu Cao Lab (Johns Hopkins Medical School, Baltimore, MD). The cells were cultured in Dulbecco's modified Eagle's media (Corning) supplemented with 10% fetal bovine serum (FBS; Sigma) and 1% antibiotics solution [penicillin (10,000 units/mL) + streptomycin (10,000 µg/mL); Gibco] at 37 ^{o}C and 5% CO_2. Both the 3T3s and NuFFs were tested for mycoplasma contamination and kept for a maximum of 3 months.

Micro-fluidic device fabrication. Silicon molds were fabricated using standard photolithography procedures. Masks were designed using AutoCAD and ordered from FineLineImaging. Molds where made by following manufacturer's instruction for SU8-3000 photoresist. Two layers of photoresist were spin coated on a silicon wafer (IWS) at 500 rpm for 7 seconds with acceleration of 100 rpm/s and 2000 rpm for 30 seconds with acceleration of 300 rpm/s respectively. After a soft bake of 4 minutes at 95 ^{o}C UV light was used to etch the desired patterns from negative photoresist to yield feature heights that were approximately 15 µm. The length of the abovementioned channels is 16.88 mm and the width is 1.46 mm.

A 10:1 ratio of PDMS Sylgard 184 silicone elastomer and curing agent were vigorously stirred, vacuum degassed, poured onto each silicon wafer and cured in an oven at 80 ^{o}C for 45 minutes. Razor blades were then use to cut the devices into the proper dimensions, inlet and outlet ports were punched using a blunt-tipped 21 Gauge needle (McMaster Carr, 76165A679). The devices were then sonicated in 100% EtOH for 15 min, rinsed with water and dried using a compressed air gun.

50 mm glass bottom petri-dishes (FlouroDish Cell Culture Dish, World Precision Instruments) were rinsed with water and then dried using a compressed air gun. The petri-dishes and PMDS devices were then exposed to oxygen plasma for 1 minute for bonding. Finally, the bonded devices were placed in an oven at 80 ^{o}C for 45 minutes to further ensure enhance bonding.

Synchronization and stiffness experiments. Cells were treated with 2 or 5 µg/mL of aphidicolin (Sigma-Aldrich, A0781) for 24 hrs to synchronize them in the G1 phase of cell cycle (Mittnacht et al, 1991). The optimal concentration and incubation period was determined using standard flow cytometry techniques (Fig. S8). To serum-starve cells, the media within the chambers were removed and the chambers were rinsed with 1X PBS 3 times. Serum-free media supplemented with 1% Pen/Strep was then injected into the chambers and left on the cells for 24 hrs.

For stiffness experiments, silicone elastomer was prepared by mixing a 1:1 weight ratio of CY52-276A and CY52-276B (Dow Corning Toray) for 3 kPa (Style et al. 2014), a 0.9:1 weight ratio of CY52-276A and CY52-276B for 12.6 kPa (Berget et al. 2016), a 1:1 weight ratio of QGel 920A and QGel 920B (Quantum Silicones) for 0.4 kPa (Gutierrez et al. 2011). In all cases the elastomer was vacuum degassed for ~5 min to eliminate bubbles, the polymer was then spin-coated onto the micro-well of the dish at 1,000 rpm for 60 s. The dish was cured overnight and resulted in a ~50 µm thick layer of silicone. The devices were then rinsed with water, dried using compressed air, plasma treated and bonded to the cell volume PDMS devices. The final devices were again placed in an 80 ^{o}C for 45 minutes to enhance the bonding.

Cell Volume Measurements. Micro-fluidic chambers were exposed to 30s oxygen plasma before being incubated with 50 µg/mL of type I rat-tail collagen (Corning; 354236) for 1 hr at 37 ^{o}C. The chambers were washed with 1X PBS before approximately 50,000 cells were injected into them. The dishes were then immersed in media to prevent evaporation. The cells were allowed to adhere for 12-18 hrs in the incubator at 37 ^{o}C with 5% CO_2 and 90% relative humidity. On the day of the experiment, 0.5 µg/mL of Alexa Fluor 555 Dextran (MW 70 kD; ThermoFisher) dissolved in media was injected into the chambers and the devices were imaged within 1-2 hrs after injection.

The cells were imaged using a Zeiss Axio Observer inverted, wide-field microscope using a 20x air, 0.8 numerical aperture (NA) objective equipped with an Axiocam 560 mono charged-coupled device (CCD) camera. The microscope was equipped with a CO_2 Module S (Zeiss) and TempModule S (Zeiss) stage-top incubator (Pecon) that was set to 37 ^{o}C with 5% CO_2 for long-time imaging. Differential interference contrast (DIC) microscopy was used to accurately capture the cell area and shape and Epifluorescent microscopy was used to measure volume. Individual cells were traced using the following algorithm.

Cell contours were segmented from the DIC and epifluorescence (Volume) channels. First, a rough contour is generated from a smoothed copy of the Epi channel where pixels darker than the background intensity are identified. Next a measure of the local contrast of the DIC channel (here high contrast regions are identified) is used to expand the contour to include small features (small lamellipodia etc.) which have low contrast in the Volume channel and may be missed. This expanded contour is used to identify the cell boundary. Inner and outer annuli are created by dilating this contour 10 and 25 pixels away from the cell (shown as green and red lines in Figure S1 (a)). The mean fluorescence intensity of the pixels between inner and outer annulus, or mean background intensity, $I_{annulus}$, is related to the total channel height. The volume boundary, shown as purple line in Figure S1(a), is created by dilating the cell

contour 20 pixels away from the cell. The local fluorescence intensity enclosed by the volume boundary, I_V, corresponds to the local height above the cell (h_2, shown in Figure 1(a), main text). The volume of the cell is then calculated as follows: $V = Channel\ Height\ \sum_{pixels\ within\ volume\ boundary} \left(1 - \frac{I_V}{I_{Annulus}}\right) \delta A$.

Every experiment on cell volume was repeated at least three times with three technical repeats corresponding to the three individual channels in the microdevice. Experiments in glass gave at least 50 single cell measurements. Softer substrates yielded smaller datasets per measurement. The sample size for volume measurements was kept over 100 single cells except for 3T3s in 0.4 kPa. This was done in order to get a normal distribution for each complete dataset"

Immunofluorescence. Immunofluorescence was carried out as described as in (Aifuwa et al, 2015). Briefly, cells were seeded at either single cell density (12,000 cells/cm^2 for 3T3s, 7,500 cells/cm^2 for NuFFs) or confluent density (75,000 cells/cm^2 for 3T3s, 60,000 cells/cm^2 for NuFFs) for 12-18 hrs and then fixed with 4% paraformaldehyde (Company) for 10 minutes. Samples were then rinsed 3 times with 1X PBS. 0.1% Triton X (Company) dissolved in PBS is then added for 10 minutes, washed 3 times with 1X PBS and then the fixed cells are blocked with 1% bovine serum albumin (company) for 1 hr at room temperature. Primary antibodies are incubated overnight in 1% BSA. Antibodies used included: YAP 63.7 (1:100; ms; SC/101199), Phospho-Myosin Light Chain 2 Thr18/Ser19 (1:100; rb; Cell Signaling Technology #3674), Anti-CD105 (1:100, Rb, Abcam ab21224), Anti-Cd90/Thy1 (1:100, Rb, Abcam ab 133350). The next day the dishes are rinsed 3 times with 1X PBS and incubated for 2 hrs in secondary antibodies with the following secondary antibodies Mouse Alexa Fluor 488, Rabbit 568, and DNA was stained using 20 ug/mL of Hoechst 33342.

Wide-field microscopy using the set-up described above was used to measure the total pMLC, YAP/TAZ, and DNA content of the cells. To obtain spatial information about pMLC we used a Zeiss LSM 800 confocal microscope equipped with a 63X oil-immersion, 1.2 (NA) objective. A 567nm laser was used to image the stained cells. Images were acquired with a resolution of 1024 x 1024, which gives a field of view of 10485.76 μm^2. We imaged the cells with confocal image stocks of total thickness of 20 μm to cover the entire height of the cells. Confocal image slices were spaced 2 μm apart and the pinhole size was 1 μm.

For each fluorescence image, we subtract the pixel intensities with mean background intensity. A binary mask is generated based on the pixel intensities of fluorescence image (for the pixel intensities within the cell region is much higher than the intensities of anywhere else), where pixels within the cell/nucleus region are marked with “1” and pixels outside the cell/nucleus are marked with “0”. By

multiplying the binary mask with actual florescence image, we can identify all the pixel values that is within the cell/nucleus. The total intensities within cell/nucleus boundary is calculated by summing up all the intensity values. The cell and nucleus boundary is then traced by Matlab routine "bwboundaries". Every traced region with total area of 1,500 pixels square or less is considered as debris or cell fragments, and, therefore, is ignored.

We utilized the pMLC channel to generate the binary mask for the cell. The traced boundary is then dilated 15 pixels away from the cell, to capture all the scattered light from epifluorescence image. The binary mask for the cell nucleus is generated based on Hoechst channel. No dilation is made on nucleus mask, to avoid overestimation of total nucleus YAP. We multiply the nucleus mask with every cell mask, to exclude all the nuclei from other cells within the same field of view. The traced boundary is shown in Fig. S1 (b).

For confocal *z* stacks, the basal layer of the cell is identified when clear stress fibers are seen (as example shown in Fig. S4 (b)). All stacks that are below the basal layer are neglected. We identified the first apical slide when the stress fibers disappear. The traced boundary of every apical slides is dilated 5 pixels (~ 1 micrometer) inside the cell, to mark the inner boundary of cortical layer (marked with pink line, Fig. S4 (c)). Cortical pMLC of one apical slide is calculated by subtracting the total PMLC intensities that within the inner boundary from the total pMLC intensity. Fig. 4(c) shows pMLC are mainly cortical, except for basal layer, where clear stress fibers can be seen. Therefore, the pMLC within the cell cytoplasm is very minimal compared to cortical pMLC.

Every experiment was repeated two times with two technical repeats on every experiment. In addition, each technical repeat consisted of at least 100 single cell measurements. The sample size for qIF aimed for at least 200 single cells with exception of two experiments on 0.4 kPa for 3T3s and NuFFs for which we obtained 80 cells and 178 cells respectively. This dataset size was targeted in order to get a normal distribution for each complete dataset. Finally, no single cells were excluded during the analysis of these datasets. The only cells excluded we those forming clusters.

Y-Compound Treatment. Cells were treated with the ROCK inhibitor Y27632 (stem cell technologies,129830-38-2) to decrease expression of pMLC, a downstream protein of the Rho/ROCK pathway. Y27632 was diluted from stock in PBS and it was used at a final concentration of 100 uM. For treatment, media was replaced with fresh media and Y27632 at the final concentration for 2hrs. Then the cells were flown into the microfluidic device for volume measurement.

Theoretical Model: Mechanical Model of the Cell

A simple mechanical model was used to predict cell shapes and volumes in the main text. Under static conditions where all forces are balanced, the hydrostatic pressure difference across the cell membrane, ΔP, is balanced by membrane tension, T, and active myosin contraction, σ_a, in the cell cortex. Mathematically, this force balance can be written as:

$$H^{-1} = \frac{2(\sigma_a h + T)}{\Delta P} \quad (1)$$

where H is the local mean curvature of cell surface; h is cortical thickness, which is around 0.5 to 1μm. The inverse of local mean curvature, H^{-1}, is the local radius of curvature, the integration of which over the cell apical surface will give the overall cell volume. This force balance condition is of the form of the classic Young-Laplace equation, which was discussed in our pervious theoretical work (Tao, et. al. 2015). If the cell is not subjected to any external mechanical forces, nor to sudden osmotic shocks, the cell membrane tension, T, remains very small when compared to $\sigma_a h$ and, therefore, can be neglected. The active myosin contraction, σ_a, depends on the concentration of phosphorylated myosin, which is reported by the light intensity of phosphorylated myosin light chain (pMLC) from the quantitative immunofluorescence experiments described in the main text. We quantified the total pMLC level in the cell, which includes the contribution from apical tension $\int \sigma_a h dA$ (Fig. 3, main text). In addition, from the confocal experiments, image intensity at different z-planes was used to report variation of $\sigma_a h$ across the apical surface. The observed cell adhesion size and shape is utilized as one of the two boundary conditions used to solve for the cell shape in Eq. (1). The force balance condition also implies cell shape and volume can be predicted if we know the myosin activity, pressure difference across the membrane, and the substrate adhesion size and shape.

For a symmetrical cell spreading in a flat circular pattern (axisymmetric), as shown in Figure S3(a), a cell surface point has the coordinate:

$$\boldsymbol{R} = (R(\theta)\cos\theta\cos\phi\,, R(\theta)\cos\theta\sin\phi\,, R(\theta)\sin\theta) \quad (2)$$

where R and θ are defined in Fig. 2a in the main text. From this parameterization, the metric tensor is:

$$\boldsymbol{g} = \begin{bmatrix} R^2 + \left(\frac{dR}{d\theta}\right)^2 & 0 \\ 0 & R^2 * \cos^2\theta \end{bmatrix} \quad (3)$$

Therefore, the local areal element is: $dA = \sqrt{\det \boldsymbol{g}}\, d\theta d\phi = R\cos\theta \sqrt{R^2 + \left(\frac{dR}{d\theta}\right)^2}\, d\theta d\phi$. The unit normal vector is: $\boldsymbol{n} = (\det \boldsymbol{g})^{-1}\left(\frac{\partial \boldsymbol{R}}{\partial \theta} \times \frac{\partial \boldsymbol{R}}{\partial \phi}\right)$, and the curvature tensor is:

$$\Theta = \begin{bmatrix} \partial_\theta\partial_\theta \boldsymbol{R}(1) & \partial_\theta\partial_\phi \boldsymbol{R}(1) \\ \partial_\phi\partial_\theta \boldsymbol{R}(1) & \partial_\phi\partial_\phi \boldsymbol{R}(1) \end{bmatrix} \boldsymbol{n}(1) + \begin{bmatrix} \partial_\theta\partial_\theta \boldsymbol{R}(2) & \partial_\theta\partial_\phi \boldsymbol{R}(2) \\ \partial_\phi\partial_\theta \boldsymbol{R}(2) & \partial_\phi\partial_\phi \boldsymbol{R}(2) \end{bmatrix} \boldsymbol{n}(2) + \begin{bmatrix} \partial_\theta\partial_\theta \boldsymbol{R}(3) & \partial_\theta\partial_\phi \boldsymbol{R}(3) \\ \partial_\phi\partial_\theta \boldsymbol{R}(3) & \partial_\phi\partial_\phi \boldsymbol{R}(3) \end{bmatrix} \boldsymbol{n}(3) \quad (4)$$

With this parameterization, the off-diagonal part of this matrix is zero and the two principle curvatures are: $c_1 = g_{11}^{-1}\Theta_{11}$ and $c_2 = g_{22}^{-1}\Theta_{22}$. The mean curvature is: $2H = c_1 + c_2$. Therefore, Equation (1) becomes:

$$H^{-1} = 2\left(\frac{2\left(\frac{dR}{d\theta}\right)^2 + R^2 - R\frac{d^2R}{d\theta^2}}{\left[R^2 + \left(\frac{dR}{d\theta}\right)^2\right]^{1.5}} + \frac{1 + \frac{dR}{d\theta}R^{-1}\tan\theta}{\sqrt{R^2 + \left(\frac{dR}{d\theta}\right)^2}} \right)^{-1} = \frac{2\sigma^a(\theta)h}{\Delta P} \quad (5)$$

This equation is a second order ODE for R as a function of θ. Thus, two boundary conditions are needed. One of the boundary conditions in this case is $R_{\theta=0} = r_0$ where r_0 is the adhesion radius. The second boundary condition is determined by the fact that the cell is smooth at the top, or, $\frac{dR}{d\theta}|_{\theta=\frac{\pi}{2}} = 0$. If $r_0 = \frac{2\sigma_a h}{\Delta P}$, the cell is a prefect hemisphere, where $\frac{dR}{d\theta} = 0$, and $H = \frac{1}{R}$. Otherwise, the cell is either flat on the top ($r_0 > \frac{2\sigma_a h}{\Delta P}$) or pinched at the bottom ($r_0 < \frac{2\sigma_a h}{\Delta P}$). Eq. (2) is solved by Matlab routine, ODE 15, which starts by assuming some initial trial solution for $R(\theta)$ and gradually changing the solution to reduce the error, $\sum_\theta \left| H^{-1} - 2\frac{\sigma_a(\theta)h}{\Delta P} \right|$ until it is close to zero.

For cells with arbitrary adhesion shapes, simple solutions of Eq. (1) are not possible and a numerical method is needed. For a triangulated surface (Fig. S3(b)), local surface mean curvature H at vertex i can be expressed as [Ref. 17 in the main text]:

$$H_i = \frac{\sum_j \left[\tan\left(\frac{\phi_{ij}}{2}\right) + \sin\left(\frac{\phi_{ij}}{2}\right)\right] l_{ij}}{4a_i} \quad (6)$$

where a_i is total area related to vertex i (the area enclosed in the green dashed line, shown in Fig. S3(b)). The sum is performed over all the neighboring vertices, j (Fig. S3(b)). ϕ_{ij} is the angle between two neighboring triangular elements that share the edge ij and l_{ij} is the edge length.

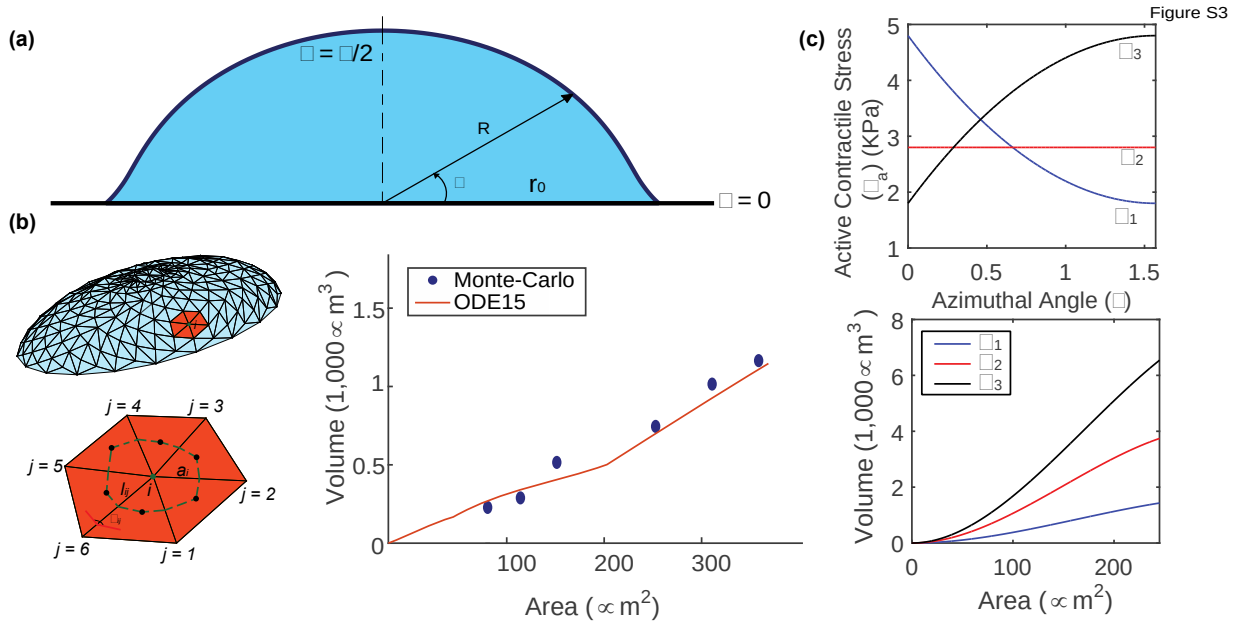

Figure S3: *Schematic description of the mechanical model; (a) Side-view of a cell adhered to a circular pattern. Here, we parametrize the surface using spherical coordinates (local radius R and azimutal angle θ, as shown in the panel). We assume the cell geometry is symmetric about $\theta = \frac{\pi}{2}$. (b) Illustration of surface triangulation. For all the triangular elements sharing the vertex i (colored in orange), j labels vertices connected to vertex i (1 to 8); a_i (Eq. (3)) is the area enclosed by the green dotted lines which perpendicularly dissect the ij edges through the center. (c) Comparison between cell volumes (V) computed from ODE 15 based on Eq. 2 (red line) and the Monte-Carlo algorithm (blue dots) for 3D cells with circular adhesions of area A. Here, $\frac{2\sigma_a}{\Delta P}h = 5\mu m$. (c). Examples of adherent area (A) vs. cell volume (V) for three different σ_a distributions. Cells with active contraction distribution similar to $\sigma_1(\theta)$ (blue line) have high basal contraction; cells with active contraction distribution similar σ_2 (read line) have uniform active contraction; cells with active contraction distribution similar to σ_3 (black line) have high apical contraction.*

While solving for cells with elliptical and equilateral triangular adhesion patterns, we utilize Eq. (3) to obtain the discrete form of Eq. (1). We solve for the cell shape by starting with an initial geometry for the cell and calculate the local mean curvature for every vertex *i*. Next, we sum the absolute errors over all the vertices: $E = \sum_i \left| H_i^{-1} - 2\frac{\sigma_{a,i}h}{\Delta P} \right|$ and take a Monte-Carlo approach, by randomly moving one vertex position at a time to minimize this total error. The cell volume from the meshed geometry is computed using Matlab code, "stlVolume", written by K. Suresh, which utilizes divergence theorem to compute the volume enclosed in a triangulated surface. (https://www.mathworks.com/matlabcentral/fileexchange/26982-volume-of-a-surface-triangulation).

To test the accuracy of the Monte-Carlo algorithm in producing cell shape and volume, we compared the cell spread area vs. cell volume computed from both the Monte-Carlo algorithm and ODE15 for axisymmetric cells spreading in a circular pattern. The cell volume computed from the Monte Carlo method agree with the solution from the ODE solver, as shown in Fig. S3 (c). We conclude that the cell geometry computed from the Monte-Carlo algorithm is reasonably accurate.

In Fig. 3 (main text), we relate the measured mean cell volume with the theoretically predicted mean volume. We calculate the mean volume of axisymmetric cells with adhesion area ranging within the measured adhesion area and with pre-assigned $\sigma_a(\theta)$, which is high in the basal region and low in apical region. From our confocal imaging, the ratio between mean apical pMLC intensity and basal pMLC intensity is used to report the ratio between mean apical σ_a and basal σ_a in our model. We multiply the measured total pMLC expression with a constant to obtain the total contractile stress: $\int \frac{\sigma_a h}{\Delta P} dA$. This constant contains a conversion factor between the observed pMLC expression and the expected mechanical stress. Our experimentally measured mean cell volumes agree with the predicted mean volumes from theory using a single conversion factor for each cell line. The fact that the conversion factor is shared across all conditions for each cell line suggests that the hydrostatic pressure difference for each cell line is a constant and spatially independent for all conditions.

Supplemental Figure Captions

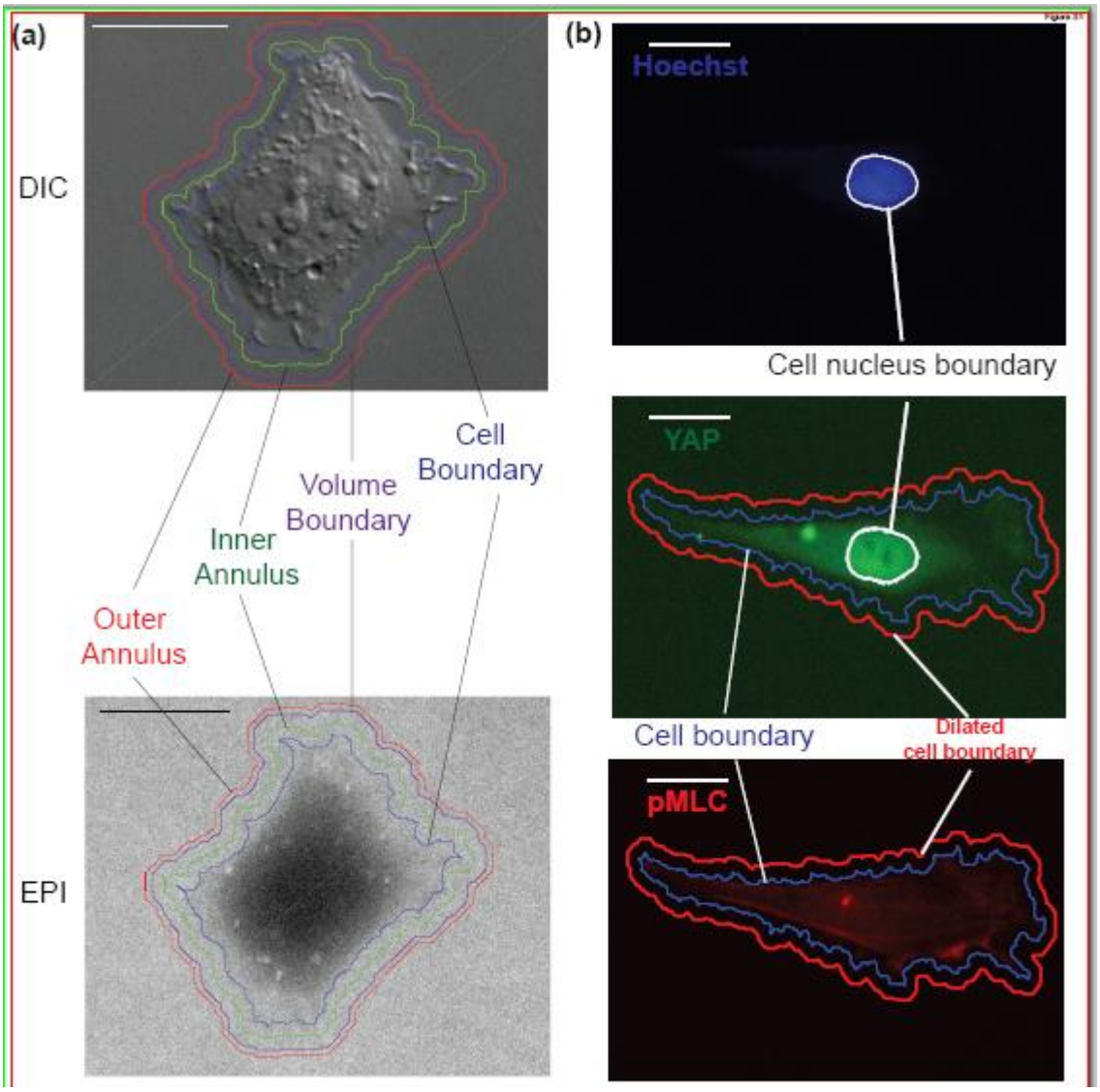

Figure S1: Quantitative immunofluorescence analysis. (a) Examples of cell images in DIC and epifluorescence channels, showing the traced cell boundary (blue), inner (green) and outer (red) annulus, and dilated boundary for volume measurement (purple) (b) Examples of traced cell boundaries from immnofluorescence images. (All scale bars = 10 micrometer.)

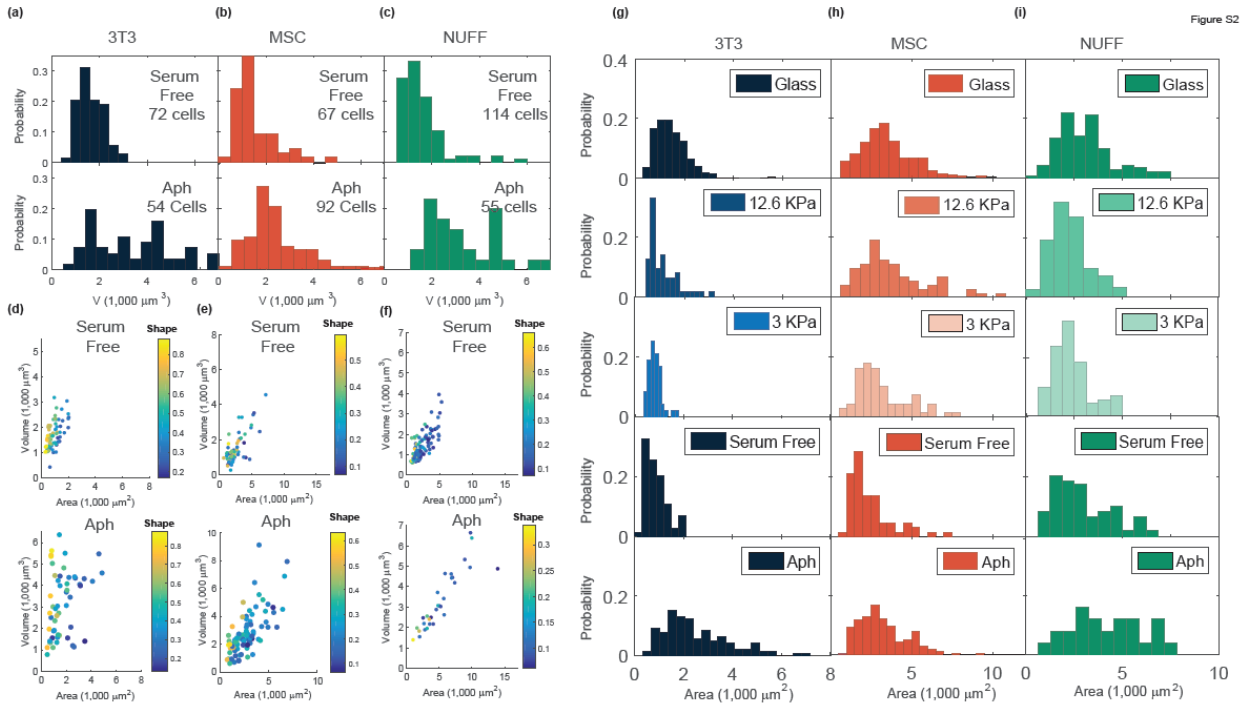

Figure S2: Volume and area data for synchronized cells. (a): Cell volume distributions for serum starvation and aphidicolin treatment of 3T3, NuFF and MSC cells seeded on glass. (b) Area vs. volume plots for serum starvation and aphidicolin treatment. (c) Distribution of cell adherent area across all three cell lines. (Number of Cells: 3T3s: N = 72 cells under serum starvation and N = 54 cells treated with Aph. MSCs: N = 67 cells under serum starvation and N = 92 cells treated with Aph. NuFFs: N = 114 cells under serum starvation and N = 55 cells treated with Aph.)

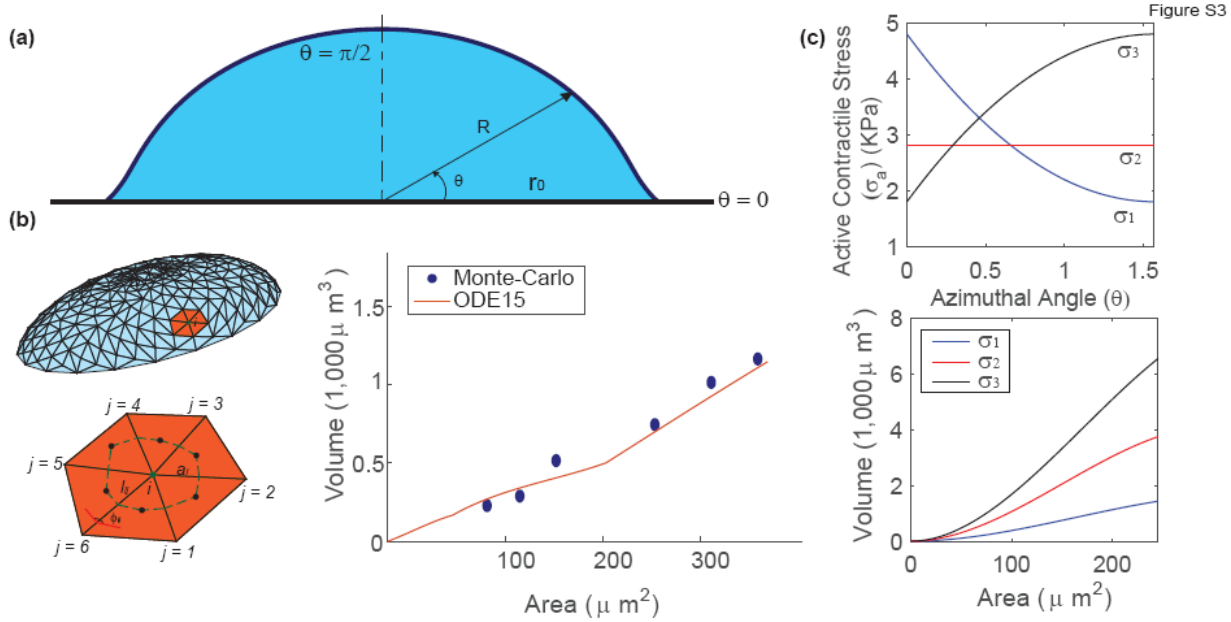

Figure S3: Schematic description of the cell mechanical model; (a) Side-view of a cell adherent on a circular pattern. Here, we parametrize the cell apical surface using a spherical coordinate system, defined by local radius R and azimutal angle θ. The surface is rotationally symmetric about the z-axis. (b) For adhered cells of arbitrary geometry, a triangulated surface in 3D is used to describe the cell apical surface. For each vertex *i*, *j* labels vertices that are connected to *i*; a_i (Eq. (3)) is the area enclosed by the green dash lines, which perpendicularly bisects the edges connecting *i* and *j*, connecting the triangle centers (marked as pink dots). We compare cell volume (*V*) vs, cell adherent area (*A*) for cells adhered to a circular pattern obtained from solving Eq. S1 using ODE15 (red line) and the 3D Monte-Carlo algorithm (blue dots). Here, $\frac{2\sigma_a}{\Delta P} h = 5\mu$m. (c). Examples of adherent area (A) vs. cell volume (V) for three different σ_a distributions. Cells with active contraction distribution similar to $\sigma_1(\theta)$ (blue line) have high basal contraction; cells with active contraction distribution similar σ_2 (read line) have uniform active contraction; cells with active contraction distribution similar to σ_3 (black line) have high apical contraction.

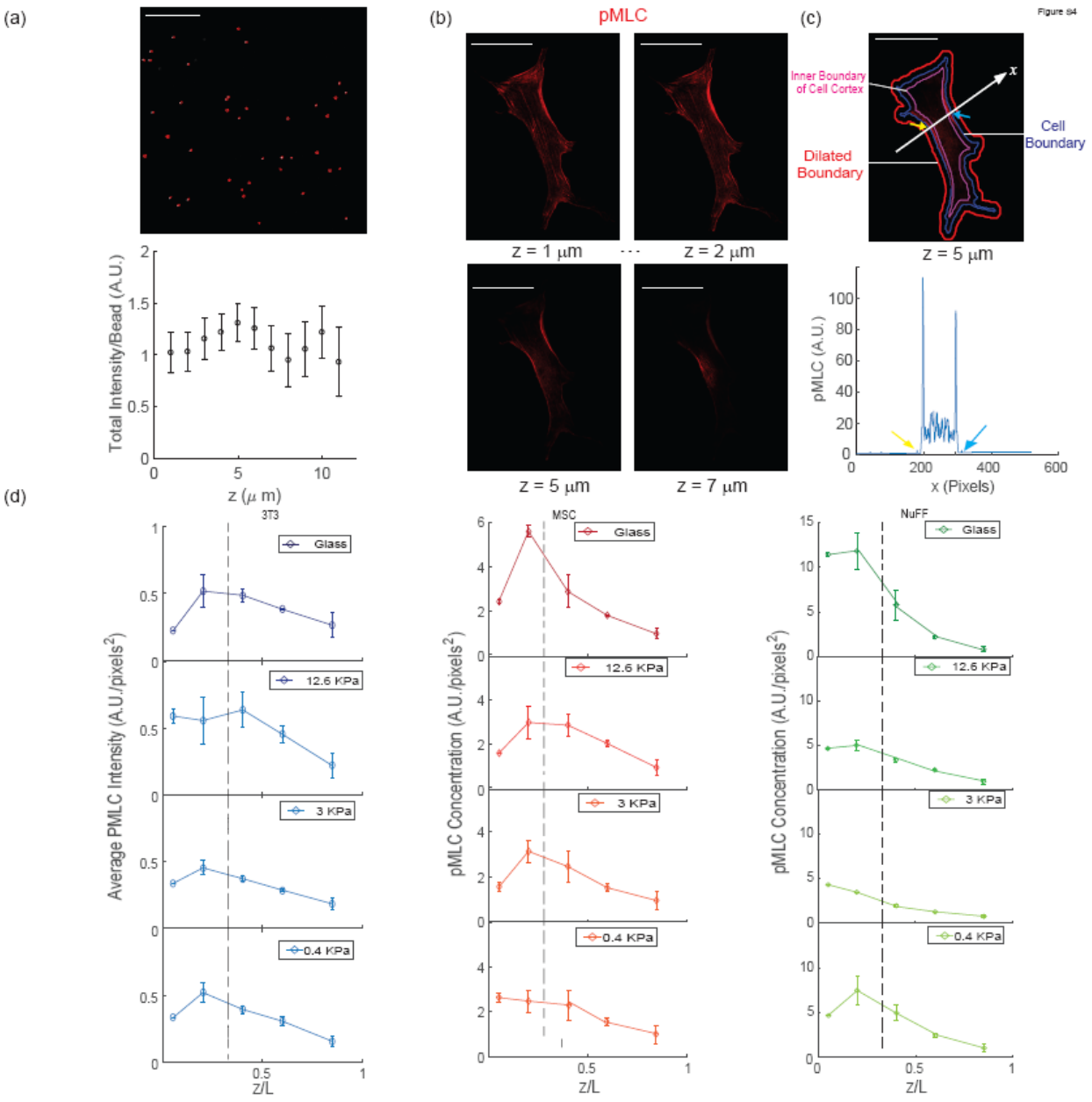

Figure S4: Quantification of spatial distribution of pMLC. (a) An example of a confocal image of fluorescent beads for one z-position. In order to calibrate our confocal intensity measurements, the total intensity per bead is plotted vs. the *z* position. The measured average intensity per bead remains roughly constant for different z-positions, demonstrating the confocal measurement can be used to quantify intensities at different z-positions. (b) Examples of confocal images of pMLC for Nuff cells on collagen-coated glass (63X): Light intensity of pMLC in the cell cortical region is much higher than elsewhere. In addition, clear stress fibers can be seen at cell basal level. (c) Example of a confocal image with the cell boundary traced by computational image analysis: the pink line marks the inner boundary of the cell cortex. The pMLC light intensity is plotted along the *x* axis (white arrow). The traced cell region is

between x = 200 to 310 pixels (marked with yellow and blue arrow, respectively). (d) pMLC intensity (total expression per united area) as a function of z-position for all three cell lines, which shows roughly the same trend as the total cortical pMLC intensity in Fig. 3 in the main text. (scale bar = 20 micrometer. All error bars represent standard error)

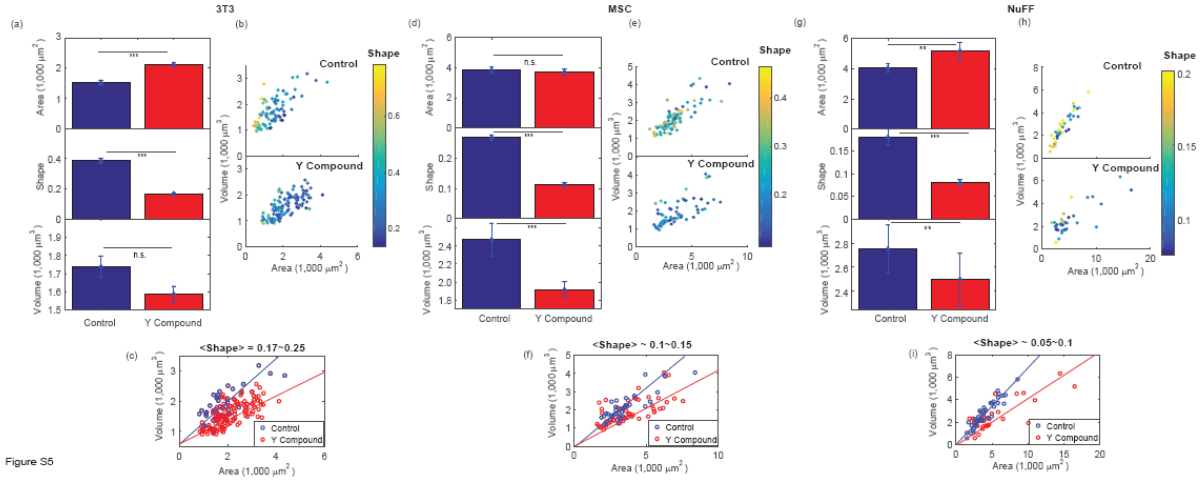

Figure S5: Cell volume after cells are exposed to ROCK inhibitor Y27632 (Y-compound) cultured on stiff glass substrate. (a), (d), and (g): cell adhesion area, shape and volume comparison between control and Y-compound treatment of 3T3 cells (a), MSC cells(d) and NuFF cells (f). (b), (e) and (h): cell adhesion area and volume plot of control and cells treated with Y27632 for 3T3s (b), MSCs, and NuFF cells (h); (c) (f) and (i): Comparison of area vs. volume plot between control and cells treated with Y27632. The comparison is done between the cells with similar shape factor. (For 3T3s: N = 94 cells for control and N = 61 cells for Y27632 treatment; For MSCs: N = 83 for control and N = 118 for Y27632 treatment; For NuFF: N = 117 for control and N = 78 for Y27632 treatment. Statistical significance; n.s. $p>0.05$; ** $p< 10^{-3}$; *** $p<10^{-6}$,.)

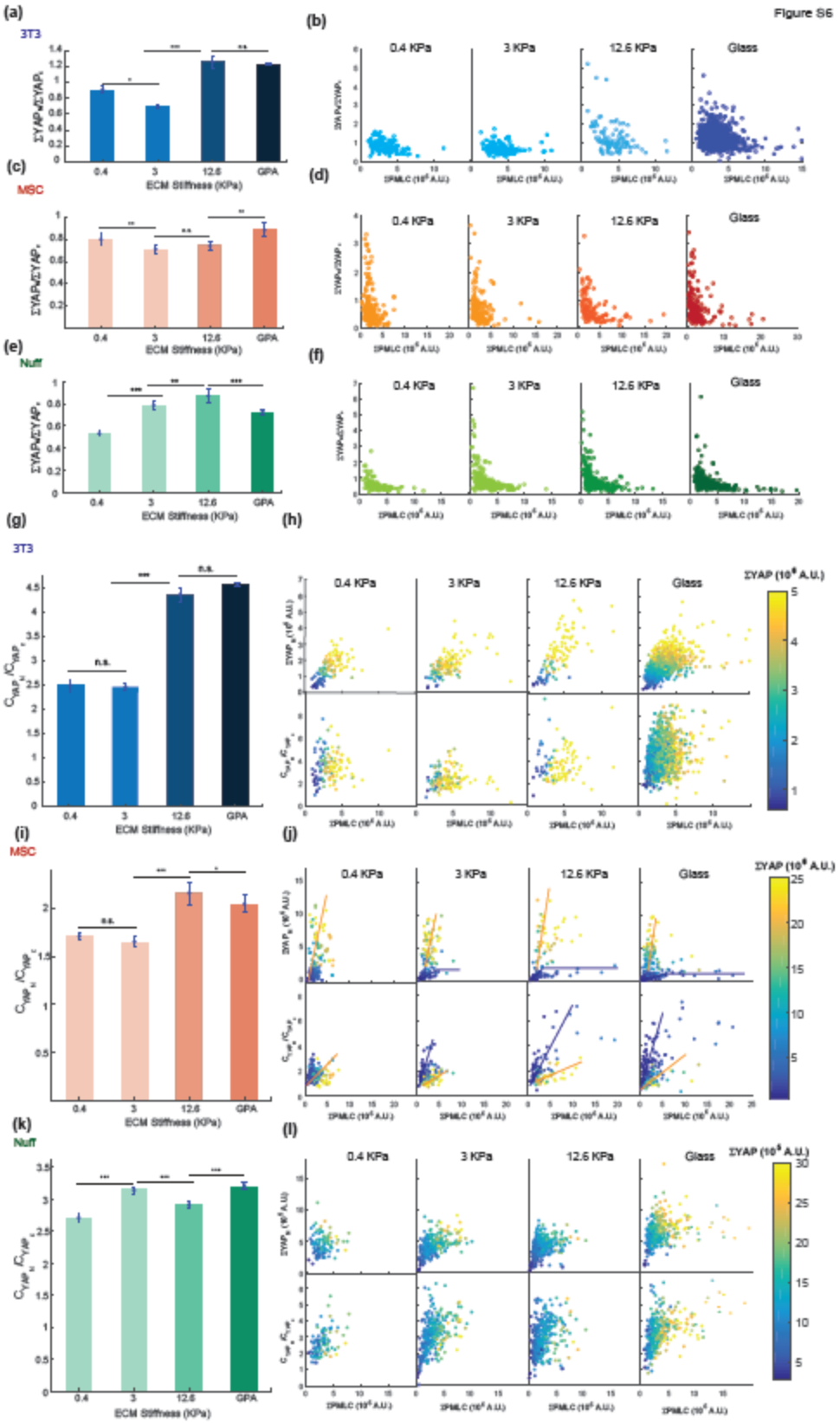
(a)
3T3
(b)
0.4 KPa
3 KPa
12.6 KPa
Glass
(c)
MSC
(d)
(e)
Nuff
(f)
(g)
(h)
(i)
(j)
(k)
(l)
ECM Stiffness (KPa)
ΣYAP (10^6 A.U.)
ΣPMLC (10^6 A.U.)
n.s.

Figure S6: Quantification of YAP distribution and pMLC from epifluorescence images. (a-f) Total pMLC intensity per cell versus the ratio between total nuclear YAP expression and total cytoplasmic YAP expression for all three cell lines. These plots show that there is no obvious correlation between pMLC and YAP ratios (a,c,e) show average value per stiffness and (b,d,f) explicitly display single cell measurements. (g-l) Correlation between total pMLC expression per cell and total nuclear YAP expression, and the correlation between total pMLC per cell and the ratio between YAP nuclear intensity and cytoplasmic intensity. (g,i,k) displays average concentration ratio per ECM stiffness and (h,j,l) Data points are color coded by the total YAP expression per cell. We find that the concentration ratio follows the trend we found between total pMLC intensity and total nuclear YAP expression. But for the MSC cells, the appearance of separate branches in the correlation is less obvious in the pMLC vs. intensity plot. Cells belong to the upper branch have high overall YAP per cell, but low nuclear to cytoplasmic YAP intensity/concentration ratio. (All error bar represent standard error. Statistical significance: *** $p<10^{-6}$, **$p< 10^{-3}$, *$p<0.01$)

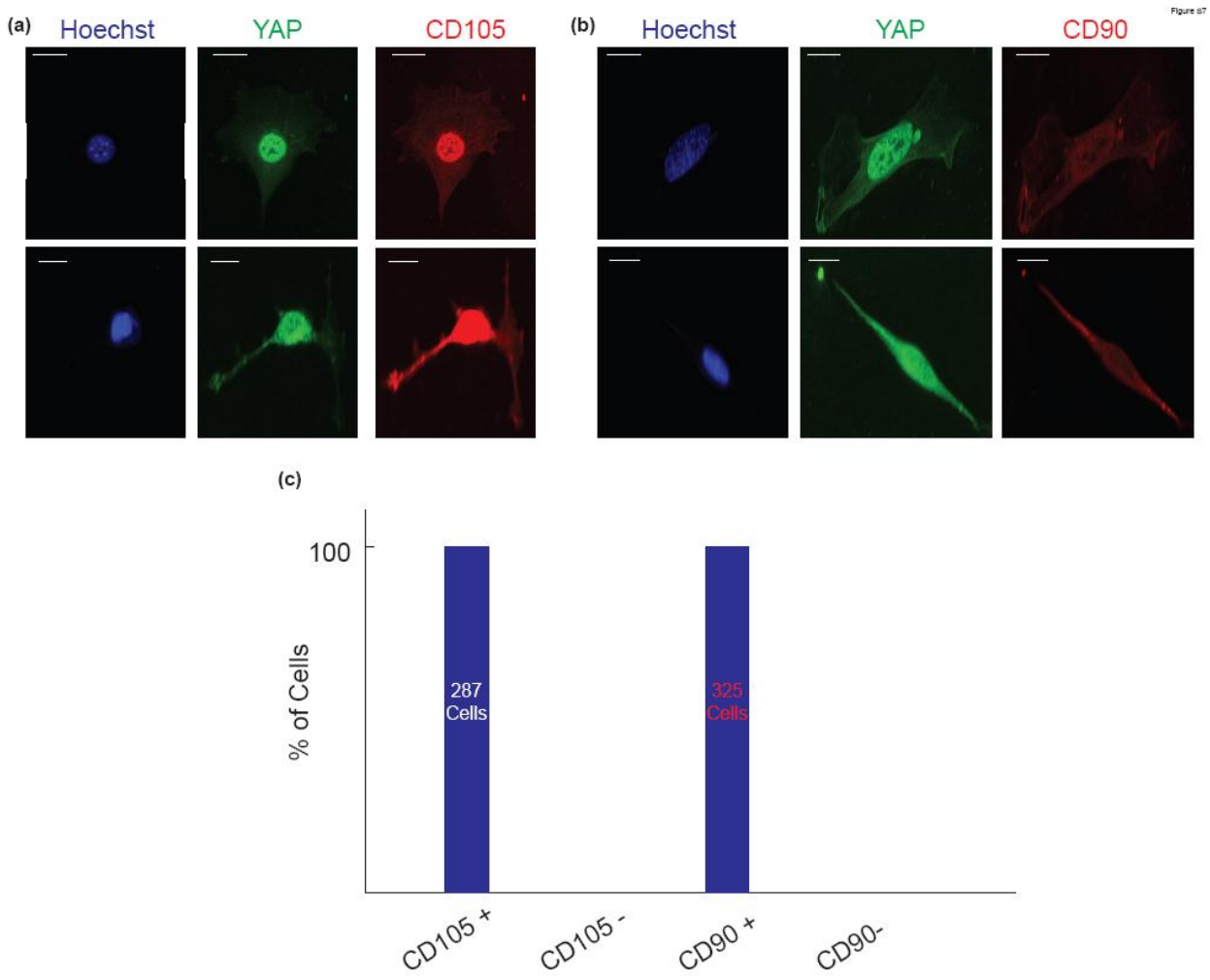

Figure S7: MSC cells expressing differential marker CD105 and CD90. All MSC cells positively express these markers.

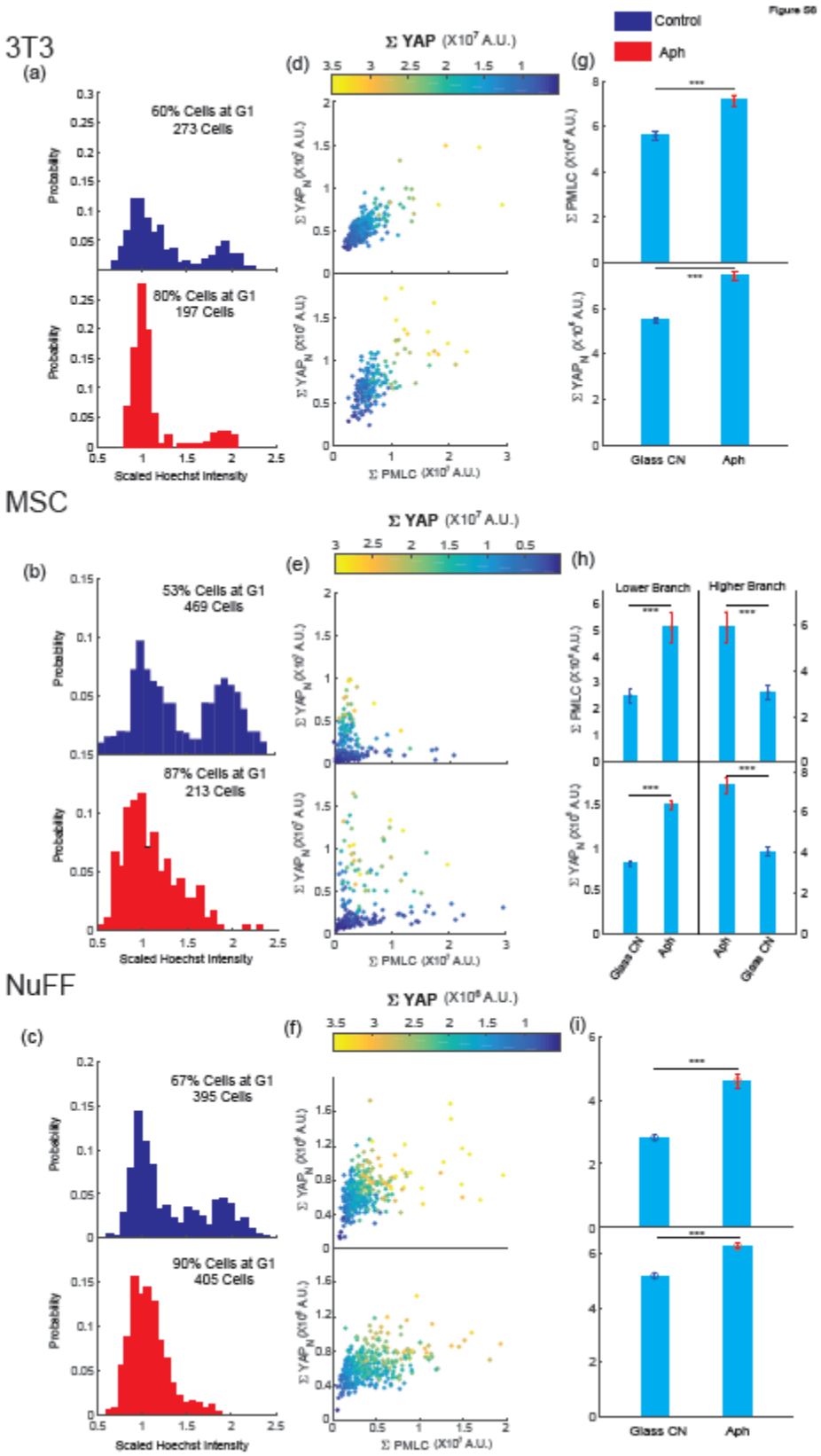
Figure S6
3T3
MSC
NuFF
(a)
(b)
(c)
(d)
(e)
(f)
(g)
(h)
(i)
60% Cells at G1
273 Cells
80% Cells at G1
197 Cells
53% Cells at G1
469 Cells
87% Cells at G1
213 Cells
67% Cells at G1
395 Cells
90% Cells at G1
405 Cells
Probability
Scaled Hoechst Intensity
Σ YAP (X10^7 A.U.)
Σ YAP (X10^8 A.U.)
Σ YAP_N (X10^7 A.U.)
Σ YAP_N (X10^8 A.U.)
Σ PMLC (X10^7 A.U.)
Control
Aph
Σ PMLC (X10^6 A.U.)
Glass CN
Aph
Lower Branch
Higher Branch
***

Figure S8: Comparisons between cells treated with aphidicolin and control for all three cell lines. (a)~(c) DNA distribution for 3T3s (a), MSCs(b),and NuFFs(c). In general, cells treated with aphidicolin are mostly in G1. (d)~(f), PMLC and YAPN plot for 3T3 (d), MSC(e) and NuFF(f) cells. (g)~(i), Comparison of mean PMLC and YAPN for 3T3 (g), MSC (h), and NuFF(i). Cells treated with aphidicolin have higher expression of pMLC and nucleus YAP. (Number of cells: 3T3s: N = 273 cells for the control and N = 197 cells treated with Aph; MSCs: N = 469 cells for the control and N = 213 cells treated with Aph. NuFFs: N = 395 cells for the control and N = 405 cells treated with Aph. *** $p<10^{-6}$,)

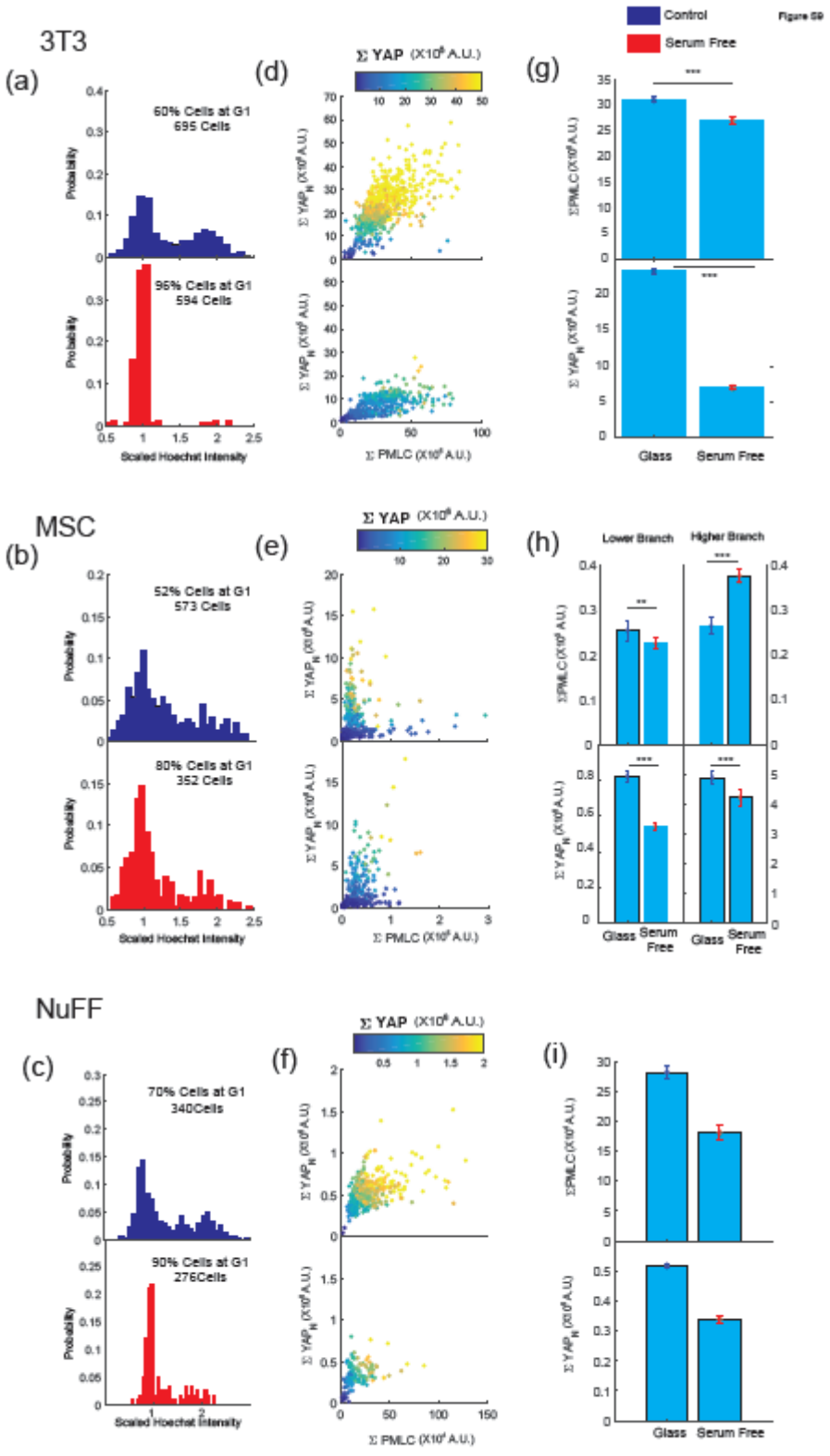
3T3
(a)
60% Cells at G1
695 Cells
96% Cells at G1
594 Cells
Probability
Scaled Hoechst Intensity
(d)
Σ YAP (X10⁶ A.U.)
Σ YAP_N (X10⁶ A.U.)
Σ PMLC (X10⁶ A.U.)
(g)
Control
Serum Free
Figure 6B
ΣPMLC (X10⁶ A.U.)
Σ YAP_N (X10⁶ A.U.)
Glass
Serum Free
MSC
(b)
52% Cells at G1
573 Cells
80% Cells at G1
352 Cells
(e)
(h)
Lower Branch
Higher Branch
Glass
Serum Free
NuFF
(c)
70% Cells at G1
340Cells
90% Cells at G1
276Cells
(f)
(i)

Figure S9: Comparisons between cells under serum free condition and control for all three cell lines. (a)~(c) DNA distribution for 3T3s (a), MSCs(b),and NuFFs(c). In general, cells cultured under serum free condition are mostly in G1. (d)~(f), PMLC and YAPN plot for 3T3 (d), MSC(e) and NuFF(f) cells. (g)~(i), Comparison of mean PMLC and YAPN for 3T3 (g), MSC (h), and NuFF(i). In general, cells cultured under serum free condition have lower pMLC and nucleus YAP, except for the higher branch of MSCs, where there are higher percentage of cells at upper branch when treated with serum free condition (Number of cells: 3T3s: N = 695 cells for the control and N = 594 cells cultured under serum free condition; MSCs: N = 573cells for the control and N = 352 cells cultured under serum free condition. NuFFs: N = 340 cells for the control and N = 276 cells cultured under serum free condition. *** $p<10^{-6}$,; ** p<=0.001)

References

Aifuwa, Ivie, et al. "Senescent stromal cells induce cancer cell migration via inhibition of RhoA/ROCK/myosin-based cell contractility." *Oncotarget* 6.31 (2015): 30516.

Bergert, Martin, et al. "Confocal reference free traction force microscopy." *Nature Communications* 7 (2016): 12814.

Gutierrez, Edgar, et al. "High refractive index silicone gels for simultaneous total internal reflection fluorescence and traction force microscopy of adherent cells." *PLoS One* 6.9 (2011): e23807.

Mittnacht, Sibylle, and Robert A. Weinberg. "G1/S phosphorylation of the retinoblastoma protein is associated with an altered affinity for the nuclear compartment." *Cell* 65.3 (1991): 381-393.

Style, Robert W., et al. "Traction force microscopy in physics and biology." *Soft matter* 10.23 (2014): 4047-4055.